Catalysis Letters Vol. 110, Nos. 1–2, August 2006 (© 2006)
DOI: 10.1007/s10562-006-0097-8

PdO/Al_2O_3–$(Ce_{1-X}Zr_X)O_2$ catalysts: effect of the sol-gel support composition

Gabriela Pérez Osorio,[a,*] Sergio Fuentes Moyado,[b] Vitalii Petranovskii,[b] and Andrey Simakov[b]

[a]*Posgrado en Física de Materiales, Centro de Investigación Científica y de Educatión Superior de Ensenada, B.C., (CICESE), Apdo. Postal 2732, Ensenada, B.C., México*

[b]*Departamento de Catálisis, Centro de Ciencias de la Materia Condensada, Universidad National Autónoma de México (UNAM), Apdo. Postal 2681, Ensenada, B. C., México*

Received 24 October 2005; accepted 23 May 2006

The contribution of $(Ce_{1-X}Zr_X)O_2$ additives to alumina supports prepared by sol-gel and the catalytic properties of PdO/Al_2O_3–$(Ce_{1-X}Zr_X)O_2$ catalysts (~0.3 wt% Pd, ~5 wt% $(Ce_{1-X}Zr_X)O_2$) in CO oxidation was herein investigated. The addition of $(Ce_{1-X}Zr_X)O_2$ to the support enhanced the surface area and decreased the size of Al_2O_3 particles. The UV–Vis bands of PdO particles and Pd^{2+} ions indicate that zirconia in $(Ce_{1-X}Zr_X)O_2$ promotes palladium-support interactions by forming highly dispersed PdO particles. Temperature-programmed reduction (TPR) in hydrogen revealed that ceria enhanced the redox capacity of the supports while zirconia lowered the reduction temperature of palladium oxide species. The comprehensive study revealed that the Ce/Zr ratio was a key factor influencing the catalytic activity of samples in CO oxidation, because palladium oxide-support interactions had a significant effect in changing of the reducibility of samples. So, the PdO/Al_2O_3–$(Ce_{0.5}Zr_{0.5})O_2$ exhibited the highest catalytic activity.

KEY WORDS: Pd oxide supported catalysts; sol-gel alumina; ceria–zirconia mixed oxides; redox behavior CO oxidation.

1. Introduction

Three-way catalysts (TWC) actually used for removal of pollution gases from automobile exhaust contain noble metals supported on mixed oxides, Pd-only TWC constitutes a new catalyst generation with improved performance compared to conventional rhodium-containing technologies due to palladium good resistance to thermal sintering [1,2]. Since the support plays a key role in the TWC performance, mixed oxides like alumina–ceria have been widely studied. Ceria acts as alumina surface area stabilizer [3] and as oxygen storage capacitor (OSC) that operates under atmospheres oscillating between rich and lean conditions, due to its ability to undergo easy the Ce^{3+}/Ce^{4+} redox process [4]. The OSC is useful to adjust the air/fuel ratio achieving a high conversion efficiency of pollutants such as CO, hydrocarbons (HC) and NO_X in the TWC [5]. Several studies have been devoted to ceria-containing materials where the presence of noble metal particles on the oxide surface promotes the OSC [6,7].

However, ceria suffer the loss of the OSC with decreasing surface area after exposing to moderate temperature treatments (above 350°C) [8]. The addition of zirconia (ZrO_2) to ceria (CeO_2) leads to a solid solution formation, which enhances ceria thermal stability by structural and redox properties modifications [8,9]. The ceria–zirconia mixed oxides prepared by different techniques like coimpregnation or cogellation offer a mutual stabilization with the alumina support [10] and promote the dispersion and catalytic activity of palladium [11,12]. The preparation method of the support and the load of zirconia play an integral role in the catalytic performance of these complex systems. The aim of this work was to characterize the PdO/Al_2O_3–$(Ce_{1-X}Zr_X)O_2$ catalysts by means of BET, XRD, TEM, DRS and H_2-TPR and examine the influence of the addition of CeO_2 and ZrO_2 in the activity for CO oxidation. The catalytic activity was compared in terms of temperature when 50% of CO is converted to CO_2 ($T_{50\%}$).

2. Experimental

2.1. Catalyst preparation

The Al_2O_3–$(Ce_{1-X}Zr_X)O_2$ supports (X = 0, 0.25, 0.33, 0.5, 0.67, 0.75, 1) were prepared by the sol-gel method. Ethanol solutions of cerium (III) acetylacetonate and zirconium (IV) acetylacetonate mixed in desired proportion were added to the solution of aluminum sec-butoxide in hexylenglycol under Ar atmosphere. The resulting sol was stirred and refluxed for 3 h at 94°C. The hydrolysis was performed by adding dropwise an appropriate amount of water. In order to

*To whom correspondence should be addressed.
E-mail: fuentes@ccmc.unam.mx

promote the gelation and aging processes, the resulting precipitate was maintained at 94°C for 10 h Drying of the gel for solvent removal involved evaporative drying in vacuum. The powder obtained was collected and calcined in flowing N_2 at 450°C for 12 h and then in air at 650°C for 4 h. The total amount of $(Ce_{1-X}Zr_X)O_2$ in the supports was 10 wt%. These supports were impregnated with aqueous solution of palladium chloride ($PdCl_2$) to achieve a 0.3 wt% metal Pd loading. The impregnated supports were dried and then re-calcined in air at 650°C for 4 h to form the PdO/Al_2O_3–$(Ce_{1-X}Zr_X)O_2$ catalysts.

2.2. Catalyst characterization

Chemical analysis of prepared samples by inductive coupled plasma (ICP) technique was done using Optical Emission Spectrometer Optima 4300 D. Before analysis sample was dissolved in sulphuric acid solution (1:1).

Specific surface area values were obtained in a Micromeritics Gemini 2360 instrument, by physical adsorption of N_2 at −196°C, using the BET equation, The samples were previously treated at 150°C under flowing Ar for 2 h.

The XRD patterns were recorded in a Philips X-Pert diffractometer using CuK_α radiation operating at 40 kV and 30 mA, and 2θ scanning from 20° to 80°, Crystalline phases were identified by comparison with ICDD reference files.

Characterization of the microstructure of catalysts was performed by high resolution transmission electron microscopy (HRTEM) in a Jeol 2010 microscope operating at 200 kV. The typical bright field images did not revealed the presence of palladium oxide nanoparticles due to the low concentration of metal (~ 0.3 wt% Pd), only by means of dark field images some PdO small particles were observed. The dark field images were obtained by selecting diffraction rings containing spots of palladium oxide and alumina. The samples were ground with a mullite mortar and were ultrasonically dispersed in isopropyl alcohol. A drop of suspension was air-dried on a carbon-coated electron microscope grid for examination.

UV–Vis diffuse reflectance spectra of catalysts in powder form packed in a quartz cell were recorded within the wavelength range 190–850 nm using a Varian Cary 300 Scan spectrometer.

Temperature-programmed reduction by hydrogen was used to get information about palladium oxide species and to monitor the reducibility of the supports and catalysts. The H_2-TPR spectra were recorded using Altamira-Ml equipment. About 0.5 g of sample was heated at 20°C/min from 25 to 550°C in flowing H_2/Ar mixture (10/190). The amount of H_2 consumed for the reduction of oxide species was measured by a thermal conductivity detector (TCD) and estimated from the integration of profiles obtained.

2.3. Catalytic test of CO oxidation

About 0.075 g of sample was packed between two layers of glass wool in a fixed bed glass U-tube reactor (i.d. 4 mm). A mixture of UHP grade of 1% CO + 1% O_2 (helium balance) at 40 ml/min was used and controlled with mass flow controllers. Catalysts were pre-oxidized *in situ* in O_2 flow at 550°C for 1 h, cooled at the same atmosphere and purged by helium at room temperature. During catalytic test the temperature was increased from 25 to 250°C at 2°C/min. Reagents and products were analyzed by gas chromatography with a SRI instrument 8610C equipped with a TCD detector and two columns of molecular sieve and silica-gel, operating at 100°C. The results were presented in terms of "light-off" curves of CO conversion versus temperature.

The CO oxidation was carried out on two series of catalysts, where first series refers to fresh samples after oxidation treatment in O_2 flow at 550°C for 1 h, Second series corresponds to redox catalysts exposed to two cycles of reduction in H_2/Ar (10/90) flow with temperature increase at 20°C/min from 25 to 550°C and intermediate re-oxidation of samples in O_2 flow at 550°C for 1 h.

3. Results and discussion

3.1. BET surface area and chemical analysis

The BET surface area of the γ-alumina was increased over 20 m^2/g by adding of the CeO_2, ZrO_2 or $(Ce_{1-X}Zr_X)O_2$ oxides (table 1). The second treatment at 650°C after impregnation of Pd leading to the PdO/Al_2O_3–$(Ce_{1-X}Zr_X)O_2$ catalysts caused a decrease of the BET surface area compared to the supports; the three samples in the middle Ce–Zr range composition (X = 0.33, 0.5 and 0.66) were less affected by this treatment (table 1). The sol-gel method used in this work developed catalysts with higher surface area (~270 m^2/g) compared to materials prepared by coimpregnation (~150 m^2/g) [10] or microemulsion (~180 m^2/g) [13] methods. Since the OSC is strongly dependent on textural properties and a high surface area is required in obtaining materials with high OSC [8] the sol-gel method is very promising for such a purpose.

The data of chemical analysis of prepared samples are summarized in table 2. The ICP analysis revealed that Ce, and Zr concentrations were lower than the nominal values used for preparation. The Ce and Zr loadings determined experimentally were situated in the range from 51 to 57 % and from 74 to 83 % of their nominal values of composition, respectively. These results indicate that the process, of hydrolysis of organic precursors during the sol-gel preparation of Al_2O_3–$(Ce_{1-X}Zr_X)O_2$ could be not fully accomplished, particularly for the case of Ce.

Table 1
Surface area of supports measured by BET and particle size of alumina (nm) obtained by Scherrer equation using analytical powder diffraction software (PC-APD)

Sample	BET (m^2/g)		Alumina average particle size (nm)[a]	
	Support	Catalyst[b]	Support	Catalyst[b]
Al_2O_3–CeO_2	271	246	3.9	4.1
Al_2O_3–$(Ce_{0.75}Zr_{0.25})O_2$	280	253	3.7	4.0
Al_2O_3–$(Ce_{0.67}Zr_{0.33})O_2$	277	260	3.7	4.0
Al_2O_3–$(Ce_{0.5}Zr_{0.5})O_2$	261	246	3.9	4.1
Al_2O_3–$(Ce_{0.33}Zr_{0.67})O_2$	270	253	3.8	3.9
Al_2O_3–$(Ce_{0.25}Zr_{0.75})O_2$	283	257	3.7	3.8
Al_2O_3–ZrO_2	267	249	3.8	4.1
Al_2O_3	239	213	4.5	4.7

[a]Average particle size determined over the most intense XRD signal (440) of the γ-alumina at 66.7°. [b]0.3 wt % Pd = 28 μmol Pd/g of catalysts.

Table 2
Analysis of Pd, Ce and Zr contents by ICP

Catalyst (O.3 wt% Pd)	Experimental Pd content (wt %)	Nominal Ce content (wt %)	Experimental Ce content (wt %)	Nominal Zr content (wt %)	Experimental Zr content (wt %)
PdO/Al_2O_3–CeO_2	0.2	8.12	4.45	0.0	< 0.007
PdO/Al_2O_3–$(Ce_{0.75}Zr_{0.25})O_2$	0.2	6.09	3.42	1.84	1.45
PdO/Al_2O_3–$(Ce_{0.67}Zr_{0.33})O_2$	0.24	5.44	3.09	2.42	2.03
PdO/Al_2O_3–$(Ce_{0.5}Zr_{0.5})O_2$	0.19	4.05	2.27	3.68	2.84
PdO/Al_2O_3–$(Ce_{0.33}Zr_{0.67})O_2$	0.2	2.67	1.37	4.95	3.68
PdO/Al_2O_3–$(Ce_{0.25}Zr_{0.75})O_2$	0.2	2.03	1.07	5.52	4.12
PdO/Al_2O_3–ZrO_2	0.18	0.0	< 0.006	7.38	5.5.
PdO/Al_2O_3	0.29	0.0	< 0.006	0.0	< 0.006

The concentration of Pd determined by ICP was identical to the nominal value only for the case of Pd/Al_2O_3. All other catalysts showed lower concentrations (~0.2 wt%). This could be attributed to a decrease of acid sites situated on the surface of alumina by effect of the Ce and Zr additives. Addition of zirconia by impregnation decreases the acid sites of alumina as reported in [14].

3.2. X-ray diffraction

The XRD patterns (figure 1) revealed peaks of the typical γ-alumina structure (JCPDS; 29-0063) for all the catalysts indicating that addition of $(Ce_{1-X}Zr_X)O_2$ do not affected its spinel structure. The calculation of alumina particle size in the catalysts by the Scherrer equation using analytical powder diffraction software (PC-APD) over the most intense signal (440) of γ-alumina at 66.7° with a standard width of 0.8, indicated that it was slightly reduced from 4.7 to less than 4 nm due to the presence of the ceria–zirconia mixed oxides (table 1). Hence, for most of the catalysts it could be concluded that $(Ce_{1-X}Zr_X)O_2$ mixed oxide is present like nano-crystallites which size is below the XRD detection limits.

The PdO/Al_2O_3–$(Ce_{0.75}Zr_{0.25})O_2$ catalysts developed two weak peaks resolved at 2θ = 29.2° and 57.3°

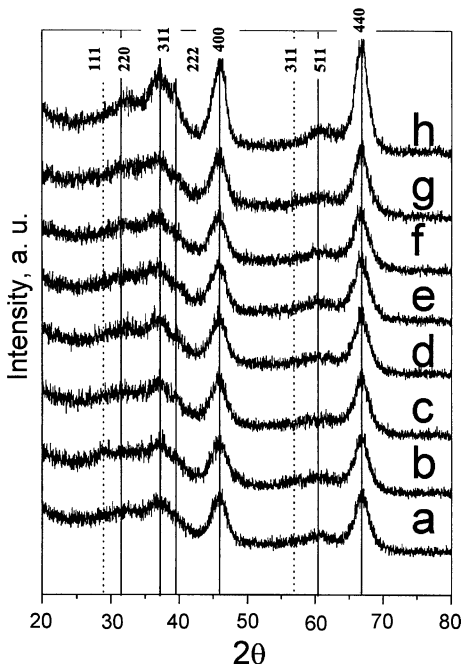

Figure 1. X-Ray diffractograms of (a) PdO/Al_2O_3–CeO_2, (b) PdO/Al_2O_3–$(Ce_{0.75}Zr_{0.25})O_2$, (c) PdO/Al_2O_3–$(Ce_{0.67}Zr_{0.33})O_2$, (d) PdO/Al_2O_3–$(Ce_{0.5}Zr_{0.5})O_2$, (e) PdO/Al_2O_3–$(Ce_{0.33}Zr_{0.67})O_2$ (f) PdO/Al_2O_3–$(Ce_{0.25}Zr_{0.75})O_2$, (g) PdO/Al_2O_3–ZrO_2, (h) PdO/Al_2O_3. Solid lines indicate γ-alumina peak positions and dotted lines indicate $Ce_{0.75}Zr_{0.25}O_2$ mixed oxide peak positions.

(figure 1, curve b) which were assigned to the most intense peaks of the $Ce_{0.75}Zr_{0.25}O_2$ cubic mixed oxide {2θ = 28.87° (111) and 2θ = 57.012° (311), (JCPDS; 28-0271)}. The shift of the (111) peak of pure cubic CeO_2 {2θ = 28.5° (JCPDS; 34-0394)} to higher angles by zirconia loading in this sample indicates the formation of a $(Ce_{1-X}Zr_X)O_2$ mixed oxide solution [10]. Evidence of palladium, cerium and zirconium oxides was not provided in the rest of the catalysts by this technique, indicating that they were well dispersed in the alumina.

3.3. Transmission electron microscopy

The ED patterns and dark field transmission electron micrographs of catalysts Pd/Al_2O_3–CeO_2, Pd/Al_2O_3–$(Ce_{0.25}Zr_{0.75})O_2$ and Pd/Al_2O_3–ZrO_2 appear in figure 2. The rings observed in the ED patterns were indexed as corresponding to the γ-Al_2O_3 phase according to data from. the X-ray Powder Data File, card No, 10–0425. The reflections (222), (400), (440), and (444) were clearly identified, other reflections were diffuse. Most of rings were broad, which suggests the presence of poorly crystallized or very small crystals of γ-Al_2O_3 phase. Nevertheless, figure 2e shows a diffraction pattern with spots assigned to the γ-Al_2O_3 phase, indicating that relatively large alumina crystal can also be formed in some cases. The dark field micrographs of those catalysts present small crystallites of alumina and some small nanoparticles of palladium oxide identified by its rounded form. The particle size of PdO was about 6 nm for PdO/Al_2O_3–CeO_2, it decreased to 3.3 nm for PdO/Al_2O_3–$(Ce_{0.25}Zr_{0.75})O_2$ and finally it increased a, little for PdO/Al_2O_3–ZrO_2 (4.5 nm). These results show that the smaller particle sizes of PdO were obtained for catalysts deposited in alumina containing $(Ce_{1-X}Zr_X)O_2$.

3.4. UV–Vis diffuse reflectance spectroscopy

The UV–Vis absorption spectra of the Al_2O_3–$(Ce_{1-X}Zr_X)O_2$ and PdO/Al_2O_3–$(Ce_{1-X}Zr_X)O_2$ samples are shown in figure 3A and B, respectively. Pure alumina (figure 3A, curve h) showed a structure-less absorption in UV with a weak band at ~260 nm, likely due to high concentration of defects in sol-gel material. In the case of the Al_2O_3–ZrO_2 sample the spectrum revealed two weak UV absorption bands at ~205 and ~260 nm, which are typical features of pure zirconia [15]. All ceria-containing samples presented an absorption edge in the near-UV region and the position slightly depended on the Ce/Zr ratio and on the presence of PdO (figure 3B). The Al_2O_3–CeO_2 sample presented a band gap energy of 3.13 eV (figure 4A), which is in agreement with the

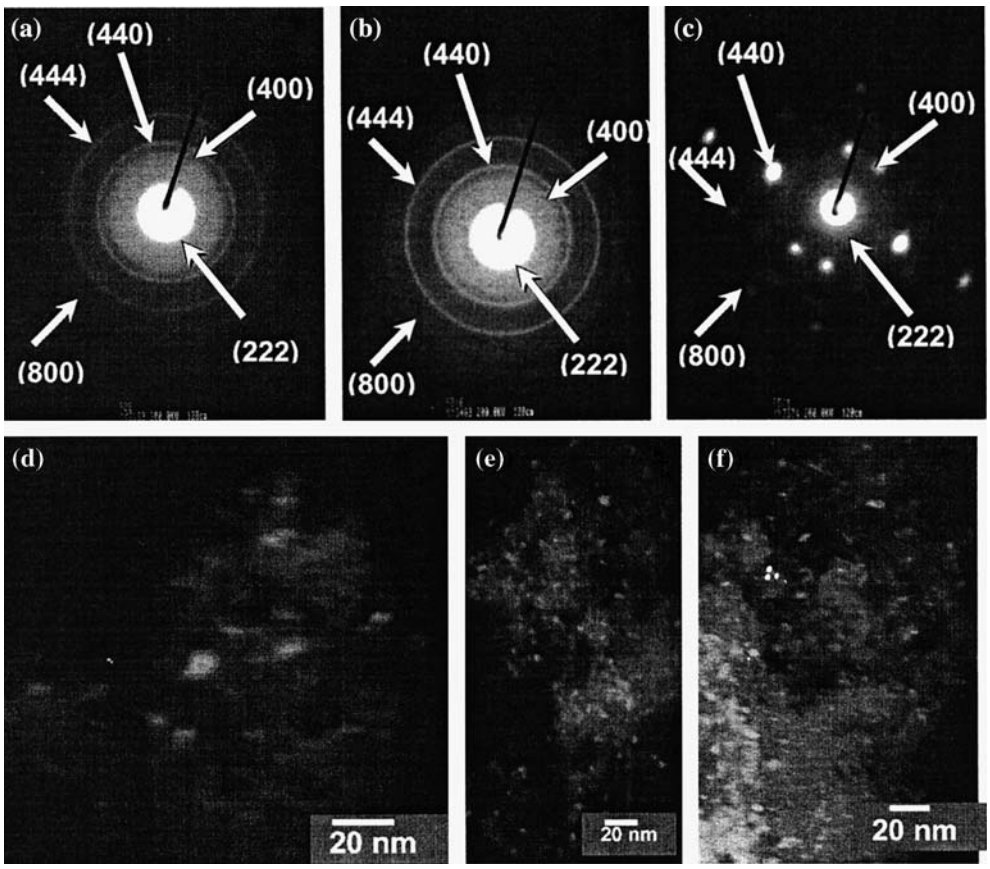

Figure 2. Electron diffraction patterns and dark field transmission electron micrographs from samples (a, d) PdO/Al_2O_3–CeO_2, (b, e) PdO/Al_2O_3–$(Ce_{0.25}Zr_{0.75})O_2$, (c, f) PdO/Al_2O_3–ZrO_2.

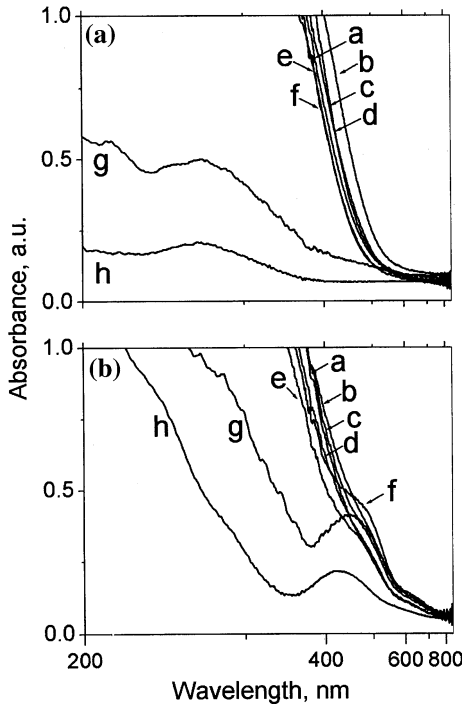

Figure 3. UV–Vis diffuse reflectance spectra for: (A) supports and (B) PdO-catalysts; denomination of samples corresponds to support compositions: (a)Al_2O_3–CeO_2, (b)Al_2O_3–$(Ce_{0.75}Zr_{0.25})O_2$, (C)Al_2O_3–$(Ce_{0.67}Zr_{0.33})O_2$, (d)Al_2O_3–$(Ce_{0.5}Zr_{0.5})O_2$, (e)Al_2O_3–$(Ce_{0.33}Zr_{0.67})O_2$, (f)Al_2O_3–$(Ce_{0.25}Zr_{0.75})O_2$, (g)Al_2O_3–ZrO_2, (h)Al_2O_3.

band-gap energy E_i value of CeO_2 thin film, reported to be 3.10 eV [16,17]. After addition of zirconia the band gap shifted down to 2.96 eV for the Al_2O_3–$(Ce_{0.75}Zr_{0.25})O_2$ sample and further it gradually shifted up with increase of the zirconia content. Addition of PdO caused a blue shift of the band gap energy for all samples, while keeping the tendency due to the increase of zirconia loading (figure 4B), Indeed, the effect of palladium oxide was much more pronounced than the effect of zirconia indicating that it can interact strongly with Ce–Zr oxides changing its electronic structure.

The PdO catalysts (figure 3B) supported on Al_2O_3 and Al_2O_3–ZrO_2 exhibit a clear absorption band between 400 and 500 nm assigned to Pd^{2+} ions and attributed to d–d transitions [18]. For ceria catalysts this band was partially masked by the absorption edge. Other two weak absorption bands associated to PdO and Pd^{2+} charge transfer [19] were observed at 224 and 283 nm (figure 5). Rise of zirconia concentration in $(Ce_XZr_{1-X})O_2$ increased the intensity of absorption bands of PdO particles and Pd^{2+} ions. Thus, zirconia promotes the palladium-support interactions by forming highly dispersed PdO particles.

3.5. *Thermal programmed reduction in hydrogen (H_2-TPR)*

Figure 6A and B present the H_2-TPR profiles of supports and palladium oxide catalysts, respectively.

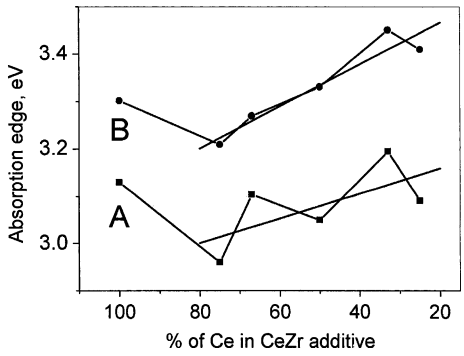

Figure 4. Dependence of band gap energy on Ce/Zr additive composition for supports (A); and palladium oxide catalysts (B).

The TPR profile of the ceria-containing supports (figure 6A) show a broad reduction peak about 430–450°C, which is indicative of the reduction of CeO_2 to Ce_2O_3 in agreement with previous reports [20,21] The use of sol-gel method had an effect in lowering of the reduction temperature of CeO_2 from 497°C [20,21] to 450 °C. The addition of Zr in the mixed Al_2O_3–$(Ce_{1-X}Zr_X)O_2$ oxides lead to an additional shift of peak maxima to $\sim$ 430°C. So, the reducibility of the supports is strongly dependent on the method of ceria loading and the addition of Zr.

The addition of palladium oxide dramatically changed the redox behavior of the samples. The TPR of the palladium oxide catalyst on alumina–ceria (figure 6B) show an intensive low-temperature peak at 180°C and a less intensive one at 340°C, similarly to other reported in [22]. The low temperature peak commonly exceeded the amount of hydrogen required to reduce the palladium oxide phase only indicating that Ce^{4+} species surrounding palladium particles are reduced too. It is suggested that palladium particles formed by reduction of PdO, in turn improve the reducibility of the supports as reported in Pd catalysts over ceria-containing supports [23]. The weak peak at high temperature ($\sim$ 400 °C) was assigned to the reduction of surface PdO complexes, which are more stable against reduction due to their strong interaction with the support [24], Then, palladium-support interactions have an effect in the significant lowering of the reduction temperature of supports [11].

The addition of zirconia to ceria led to the appearance and development of a new peak at $\sim$ 100 °C which could be assigned to the reduction of bulk PdO particles which are not interacting with the support and that are reduced at lower temperatures as in the case of catalysts of palladium oxide on alumina [25].

The varying of support composition led to different palladium oxide species, which are reduced at different temperatures. It is suggested that palladium-support interactions are enhanced by the sol-gel preparation method and controlled by the Ce/Zr ratio. It was observed that the peaks for NO reduction were wider than those of other Pd catalysts prepared by different methods [11]. This is attributed to a larger interaction of

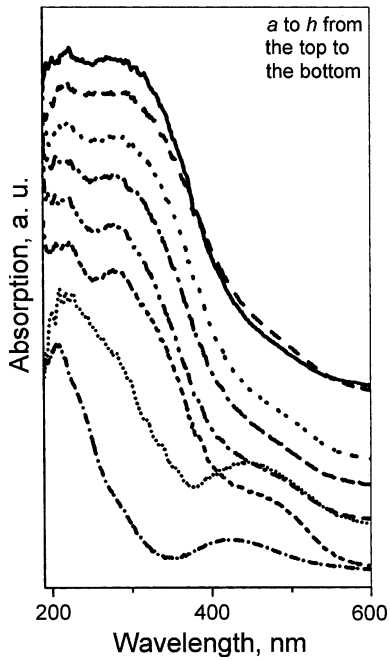

Figure 5. Diffuse reflectance spectra demonstrates gradual development of PdO bands while zirconia loading is increased. Curves are shifted for clarity. Catalysts composition (from top to bottom): (a) PdO/Al_2O_3–CeO_2, (b) PdO/Al_2O_3–$(Ce_{0.75}Zr_{0.25})O_2$, (c) PdO/Al_2O_3–$(Ce_{0.67}Zr_{0.33})O_2$, (d) PdO/Al_2O_3–$(Ce_{0.5}Zr_{0.5})O_2$, (e) PdO/Al_2O_3–$(Ce_{0.33}Zr_{0.67})O_2$, (f) PdO/Al_2O_3–$(Ce_{0.25}Zr_{0.75})O_2$, (g) PdO/Al_2O_3–ZrO_2, (h) PdO/Al_2O_3.

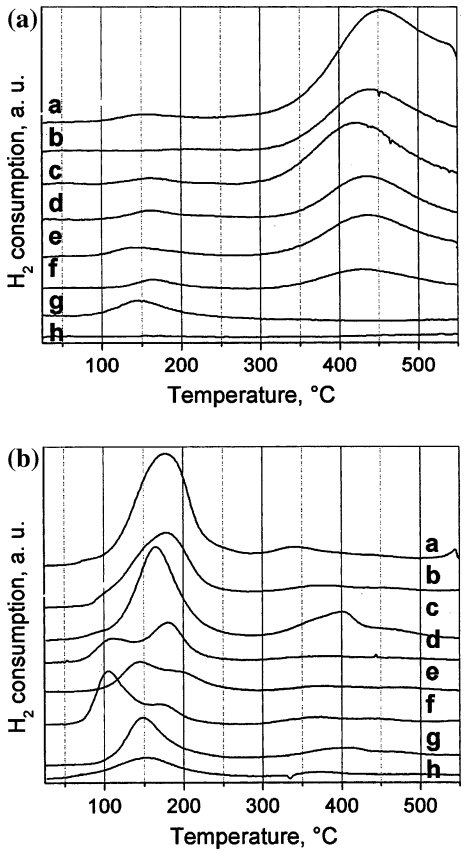

Figure 6. TPR profiles for: (A) supports and (B) PdO-catalysts; denomination of samples corresponds to support compositions: (a) Al_2O_3–CeO_2, (b) Al_2O_3–$(Ce_{0.75}Zr_{0.25})O_2$, (c) Al_2O_3–$(Ce_{0.67}Zr_{0.33})O_2$, (d) Al_2O_3–$(Ce_{0.5}Zr_{0.5})O_2$, (e) Al_2O_3–$(Ce_{0.33}Zr_{0.67})O_2$, (f) Al_2O_3–$(Ce_{0.25}Zr_{0.75})O_2$, (g) Al_2O_3–ZrO_2, (h) Al_2O_3.

PdO with highly dispersed phases of Ce–Zr in alumina obtained by the sol-gel method.

The data of the H_2 uptake during TPR runs for supports and catalysts are summarized in table 3. The hydrogen uptake measured for the supports increases proportionally to the ceria content. Estimation of hydrogen uptake permits to conclude that only about 40% of ceria could be reduced from Ce^{4+} to Ce^{3+} in TPR runs probably due to diffusion limitations. The alumina support was not reduced; meanwhile the zirconia–alumina support was only very slightly reduced. Consumption of hydrogen seems to proceed due to reaction of some organic residuals in this sample with hydrogen. The hydrogen uptake for the palladium supported catalysts increases as a function of ceria content and goes through a maximum at $X = 0.25$. Such enhanced reducibility of the catalyst with $X = 0.25$ is attributed to the formation of $(Ce_{0.75}$–$Zr_{0.25})O_2$ crystalline phase detected by X-ray diffraction. Besides, it results in a clear influence of zirconia in the redox behavior of the systems studied.

The fraction of reduced PdO can be estimated from the TPR experiments by taking into account the difference between hydrogen uptakes of catalysts and supports (table 3). For catalysts PdO/Al_2O_3, PdO/Al_2O_3–ZrO_2 and PdO/Al_2O_3–$(Ce_X$–$Zr_{1-X})O_2$ with $X = 0.75$, 0.67 and 0.25, it was estimated that PdO was totally reduced during the TPR experiment (100% reduction). For catalysts PdO/Al_2O_3–$(Ce_X$–$Zr_{1-X})O_2$ with $X = 0.5$ and 0.33, the estimated fraction of reduced PdO was ~75–80%, indicating that hard-to-reduce species were formed in that intermediate range of composition. The lower amount of reduced PdO (30% reduction) was observed for the PdO/Al_2O_3–CeO_2 catalyst, nevertheless, in this case uncertainty arises in the calculation because the TPR profile of the support remained very high from baseline indicating that CeO_2 species reduced at high temperature still remained to be taken into account at the end of the experiment, It implies that estimations for this sample characterizing with so wide peaks in TPR profiles can not be correct enough.

The TPR experiments lead to conclude that for all catalyst except PdO/Al_2O_3–CeO_2 most of PdO species were reduced in presence of hydrogen in the temperature range from 70 to 550°C. Indeed, for catalysts PdO/Al_2O_3–$(Ce_X$–$Zr_{1-X})O_2$ with $X = 0.5$ and 0.33, some hard-to-reduce PdO species were formed.

3.6. CO oxidation

Figure 7 shows light-off curves for fresh catalysts displaying the gradual increase of CO conversion from room temperature to 150 °C for all ceria containing

Table 3
Hydrogen uptake of supports and catalysts during TPR in hydrogen from ambient to 550°C and estimated fraction of reduced PdO

Catalyst	Support H_2 uptake (μmol/g)	Catalyst H_2 uptake (μmol/g)	Difference of catalyst and support H_2 uptake(μmol/g)	Amount of H_2 required to reduce PdO (μmol/g)
PdO/Al_2O_3–CeO_2	87.0	93.1	6.1	18.7
PdO/Al_2O_3–$(Ce_{0.75}Zr_{0.25})O_2$	59.0	106.5	47.5	18.7
PdO/Al_2O_3–$(Ce_{0.67}Zr_{0.33})O_2$	56.8	91.4	34.6	22.4
PdO/Al_2O_3–$(Ce_{0.5}Zr_{0.5})O_2$	37.1	52.7	15.6	17.7
PdO/Al_2O_3–$(Ce_{0.33}Zr_{0.67})O_2$	35.5	42.7	7.2	18.7
PdO/Al_2O_3–$(Ce_{0.25}Zr_{0.75})O_2$	19.2	43.3	24.1	18.7
PdO/Al_2O_3–ZrO_2	6.0	36.9	30.9	16.8
PdO/Al_2O_3	0.0	27.2	27.2	27.1

catalysts and revealing its beneficial effect. The best catalysts were those situated around middle of the Ce–Zr composition range with a $T_{50\%}$ of CO conversion at 100°C. The PdO/Al_2O_3–ZrO_2 and PdO/Al_2O_3 catalysts presented the lowest activity with CO oxidation starting at 75 °C. Indeed all catalysts reached 100% of conversion before 200°C, The ceria–zirconia additive enhanced the activity of PdO/Al_2O_3–$(Ce_X$–$Zr_{1-X})O_2$ catalysts, compared with those based on individual oxide supports. These catalysts containing ceria besides of exhibiting high catalytic activity also presented similar behavior with temperature. It has been reported that ceria plays a key role in CO oxidation by supplying oxygen to the Pd–Ce interface [26]. The highest CO conversion achieved with catalysts PdO/Al_2O_3–$(Ce_{0.5}Zr_{0.5})O_2$, PdO/Al_2O_3–$(Ce_{0.33}Zr_{0.67})O_2$ and PdO/Al_2O_3–$(Ce_{0.75}Zr_{0.25})O_2$ correlates with the highest oxygen mobility for Ce–Zr system with similar composition reported in reference [27].

The redox pretreatment slightly modified catalytic properties of catalysts in CO oxidation, as shown in figure 8, In the case of PdO/Al_2O_3–CeO_2 and PdO/Al_2O_3 the catalytic activity was diminished, on the other hand, PdO/Al_2O_3–$(Ce_{0.5}Zr_{0.5})O_2$ and PdO/Al_2O_3–$(Ce_{0.33}Zr_{0.67})O_2$ catalysts increased their activity by achieving $T_{50\%}$ of CO conversion at 92 instead of 100°C. The redox PdO/Al_2O_3 catalysts exhibited the lowest activity. The light-off profiles of redox catalysts was very similar to those of fresh catalysts and manifested the same tendency with respect to Ce/Zr ratio, except that some of them were shifted to lower temperatures. This behavior indicates that the same palladium state is obtained after redox treatment. So, the effect of redox treatment enhancing the activity of Ce–Zr catalysts could be attributed to an increase of dispersion of palladium oxide species.

The synergistic effect of Ce on PdO/Al_2O_3–CeO_2 catalysts enhancing the activity in CO oxidation is well established. The addition of zirconia to ceria also is beneficial for PdO/Al_2O_3–$(Ce_X$–$Zr_{1-X})O_2$ catalysts. This effect in turn allows stabilize palladium oxide in active state probably due to higher interaction with Ce–Zr oxides.

The higher catalytic activity of sol-gel samples reported in this work compared to samples reported by other methods is attributed with a better distribution of Ce and Zr in alumina at the nanoscale size.

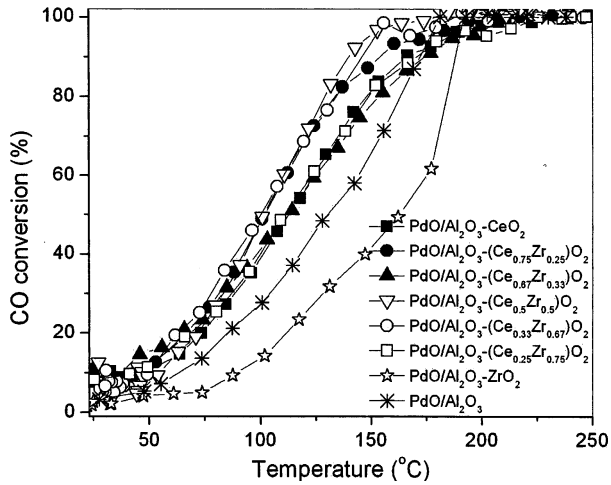

Figure 7. CO conversion profiles for the CO + O_2 reaction on fresh catalysts

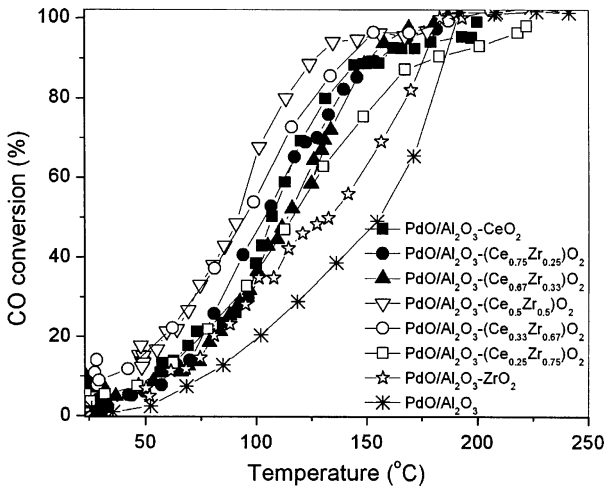

Figure 8. CO conversion profiles for the CO + O_2 reaction on redox catalysts

4. Conclusions

The addition of $(Ce_{1-X}Zr_X)O_2$ to alumina by sol-gel preparation method did not modify its typical structure but promotes an increase of the surface area. In accordance with particle size measurements, these mixed oxides also reduce the particle size of alumina. We assume that, it was a result of the introduction of Ce and Zr ions, which avoid growth of alumina crystallites during thermal treatments by forming structural defects.

The ceria-containing samples present an absorption edge in the near-UV region. The band gap energy depends both on the Ce/Zr ratio and the presence of PdO, indicating changes in the electronic structure of the catalysts. Increasing of the zirconia content in $(Ce_{1-X}Zr_X)O_2$ promotes the palladium-support interactions by formation of highly dispersed PdO species.

The reducibility of the supports is strongly dependent on the ceria loading. Palladium-support interactions promoted by sol-gel preparation method have an effect in lowering the reduction temperature of the catalysts and are controlled by the Ce/Zr ratio, The species of palladium oxide depend on the Ce/Zr ratio of the supports.

The presence of palladium oxide interacting with Al_2O_3–$(Ce_{1-X}Zr_X)O_2$ system improves the CO oxidation and the Ce/Zr ratio is a key factor influencing the activity. The PdO/Al_2O_3–$(Ce_{0.5}Zr_{0.5})O_2$ exhibits the highest catalytic activity in agreement with results reported on PdO supported on bulk $(Ce_{0.5}Zr_{0.5})O_2$ oxides [27]. The same reason assumed in that report for the increase of activity, which is the improved mobility of oxygen in Ce–Zr oxides, is also assumed in this work. The improved activity of PdO/Al_2O_3–$(Ce_{0.5}Zr_{0.5})O_2$ obtained by sol-gel with respect to reported studies of $Pd/(Ce_{0.5}Zr_{0.5})O_2$ is attributed to the enhanced dispersion of the Ce–Zr oxides within alumina. Further studies are in process in order to elucidate the type of interaction between palladium oxide species and the Al_2O_3–$(Ce_{1-X}Zr_X)O_2$ supports.

Acknowledgments

This research project was supported by CONACyT México through Grant No. 41331-Y: The authors acknowledge Eloisa Aparicio, Eric Flores, Pedro Casillas, Margot Sainz and Juan A. Peralta for their technical support. G. Pérez is grateful to Drs. Miguel Angel Hernández and Hugo Tiznado for helpful suggestions and CONACyT for scholarship No. 122975.

References

[1] J.C. Summers and W.B. Williamson, in: Environmental Catalysis, ACS Symp. Ser., Vol. 552, ed. J.N. Armor (Am. Chem. Soc. Washington, DC, 1994) p. 94.
[2] R.M. Heck and R.J. Farrauto, in: Catalytic Air Pollution Control (International Thomson Publishing, New York, 1995) p. 102.
[3] A. Piras, A. Trovarelli and G. Dolcetti, Appl. Catal. B 28 (2000) L77.
[4] V. Perrichon, A. Laachir, G. Bergeret, R. Frety, L. Tournayan and O. Touret, J. Chem. Soc. Faraday Trans. 90 (1994) 773.
[5] G.Y. Adachi and T. Masui, in: Catalysis by Ceria and Related Materials, ed. A. Trovarelli (Imperial College Press, London, 2001) p. 51.
[6] S. Bedrane, C. Descorme and D. Duprez, Catal. Today 75 (2002) 401.
[7] C. Descorme, R. Taha, N. Mouaddib-Moral and D. Duprez, Appl. Catal. A 223 (2002) 287.
[8] P. Fornasiero, G. Balducci, R. Di Monte, J. Kaspar, V. Sergo, G. Gubitosa, A. Ferrero and M. Graziani, J. Catal. 164 (1996) 173.
[9] M. Boaro, M. Vicario, C. de Leitenburg, G. Dolcetti and A. Trovarelli, Catal. Today 77 (2003) 407.
[10] A.I. Kozlov, D.H. Kim, A. Yezerets, P. Andersen, M.C. Kung and H.H. Kung, J. Catal. 209 (2002) 417.
[11] M.F. Luo and X.M. Zheng, Appl. Catal. A 189 (1999) 15.
[12] C. Bozo, N. Guilhaume and J.M. Herrman, J. Catal. 203 (2001) 393.
[13] M. Fernández-García, A. Martínez-Arias, A. Iglesias-Juez, C. Belver, A.B. Hungría, J.C. Conesa and J. Soria, J. Catal. 194 (2000) 385.
[14] H.R. Chen, J.L. Shi, T.D. Chen, J.N. Yan and D.S. Yan, Mater. Lett. 54 (2002) 200.
[15] H. Tiznado, S. Fuentes and F. Zaera, Langmuir 20 (2004) 10490.
[16] C.A. Hogarth and Z.T. Al-Dhhan, Phys. Stat. Sol. B 137 (1986) K157.
[17] T. Masui, K. Fujiwara, K.-I. Machida, G.-Y. Adachi, T. Sakata and H. Mori, Chem. Mater. 9 (1997) 2197.
[18] A.S. Sass, V.A. Shvets, G.A. Savelyeva and V.B. Kazanskii, Kinet. Catal. 26 (1985) 1149.
[19] A.N. Pestryakov, V.V. Lunin, S. Fuentes, N. Bogdanchikova and A. Barrera, Chem. Phys. Lett. 367 (2003) 102.
[20] H.C. Yao and Y.F.Y. Yao, J. Catal. 86 (1984) 254.
[21] A. Trovarelli, Catal. Rev. Sci. Eng. 38 (1996) 439.
[22] A. Trovarelli, G. Dolcetti, C. de Leitenburg, J. Kaspar, P. Finetti and A. Santoni, J. Chem. Soc. Faraday Trans. 88 (1992) 1311.
[23] E. Bekyarova, P. Fornasiero, J. Kaspar and M. Graziani, Catal. Today 45 (1998) 179.
[24] H. Lieske and J. Völter, J. Phys, Chem. 89 (1985) 1841.
[25] R.S. Monteiro, F.B. Noronha, L. Ch. Dieguez and M. Schmal, Appl. Catal. A 131 (1995) 89.
[26] M. Fernández-García, A. Martínez-Arias, L.N. Salamanca, J.M. Coronado, J.A. Anderson, J.C. Conesa and J.C. Soria, J. Catal. 187 (1999) 474.
[27] M. Boaro, C. de Leitenburg, G. Dolcetti and A. Trovarelli, J. Catal. 193 (2000) 338.